Modeling and Applications of a Chemical-Loaded UHF RFID Sensing Antenna With Tuning Capability

Sabina Manzari, *Student Member, IEEE*, and Gaetano Marrocco, *Member, IEEE*

***Abstract*—A key-issue of the wireless gas sensing by radio frequency identification is the capability to control the sensor's response while minimizing the amount of chemical interactive materials (CIM) required to dope the tag antenna. An open-circuit shielded slot-line layout is proposed as a general purpose tunable radio frequency identification (RFID) radiator, suitable to host small amounts of CIM. It operates both as a very efficient passive sensor and as a tool to estimate the electromagnetic equivalent parameters of the CIM during the gas exposure. A hybrid distributed-lumped model permits to separate the CIM's contribution from the antenna's response and, in addition, it provides a simple tool to shape the calibration curve relating RFID power signals to the physical changes of the environment. The tag layout and the method are applied to the UHF characterization of the conductive polymer Pedot:PSS and to the optimization of high-performance humidity sensor capable of a three-times higher sensitivity than those achieved by the current state of the art RFID devices.**

***Index Terms*—Chemical interactive material, humidity, radio frequency identification (RFID), sensor, slot-line.**

I. Introduction

THE ongoing devolution of Internet technology towards the real world [1] is stimulating a remarkable research interest on wireless devices for sensing chemical species within heterogeneous environments, such as farms, hospitals, domestic places, and even agriculture fields ([2]–[6]). In spite of the wide utilization of battery-assisted nodes, the true pervasive distribution of wireless sensors will be really pushed by completely passive devices, due to the reduced cost and the absence of maintenance. In this scenario, the potentiality of ultrahigh frequency (UHF) radio frequency identification (RFID) technology able to provide sensing features is currently investigated by many researchers worldwide. The physical rationale [7] is that the response of a passive antenna to an incoming electromagnetic field emitted by a remote unit (the reader) can be modulated by means of lumped or even distributed loading of the antenna with specialized chemical interactive materials (CIM). These receptors will experience changes of their dielectric properties through interaction with target molecules [8] and, in turn, will induce a variation of antenna's impedance and gain. Some early experiments with augmented UHF RFID passive tags and even with chipless tags demonstrated the possibility to detect the presence of toxic gases and humidity in air [9]–[13].

Such papers demonstrated the proof of the concept for passive gas sensing. However, some key issues are still in question, such as techniques to minimize the amount of the CIM needed while maximizing sensitivity and communication performance, the control over the response of the radio-sensor and the cross-sensitivity to multiple physical parameters. Moreover, the CIMs are mostly characterized only in DC [14] and hence the design of these antennas suffers from the lack of information about the CIM's electromagnetic parameters in the UHF RFID band.

A possible approach to RFID *sensing engineering* is to describe the complex interactions between CIM, antenna and volatile compounds as simple lumped-element circuits, that is possible when the loading CIM is a very localized displacement. In this view, a first idea about how achieving remarkable sensing capability by using a single CIM drop, was very recently anticipated by the authors in [15]. It was experimentally demonstrated how a single polymer drop of "PEDOT: PSS" (poly (3,4-ethylenedioxythiophene):poly (styrenesulfonic acid) [16] placed inside a radiating slot of a proper tag layout is capable to magnify the effect of electrical changes over the tag's impedance. Starting from above laboratory evidence, this paper further investigates that idea up to develop a general purpose electromagnetic model of the drop-loaded tag, which can be useful to support the design of effective chemical radio-sensors and, at the same time, to easily estimate the electromagnetic UHF parameters of the specific CIM during gas exposure.

As in [15], the considered tag employs a slot-line layout and a tuning mechanism able to shift the antenna response at each frequency of the global UHF RFID band (865–928 MHz). This feature is hence potentially useful to modify the dynamic range of the sensor and its sensitivity, as detailed later on. The CIM is assumed to be placed into a small $((\lambda)/(100) \times (\lambda)/(100))$ niche and a lumped element model is introduced to mathematically separate the effect of the CIM from the response of the unloaded (blank) tag. The gas sensing application and CIM characterization are illustrated experimentally by using PEDOT:PSS as CIM for humidity detection, since some references and comparing informations are available from recent papers, previously listed.

The paper is organized as follows. Section II introduces the antenna layout and the control parameters. A lumped model of the chemical loaded device, used to estimate the power transfer coefficient and realized gain, is described in Section III. Section IV shows an experimental prototype and some comparisons between simulations and measurements

Manuscript received March 05, 2013; revised July 30, 2013; accepted September 22, 2013. Date of publication October 23, 2013; date of current version December 31, 2013.

The authors are with the University of Roma Tor Vergata, 00133 Rome, Italy (e-mail: manzari@disp.uniroma2.it; gaetano.marrocco@uniroma2.it).

Digital Object Identifier 10.1109/TAP.2013.2287008

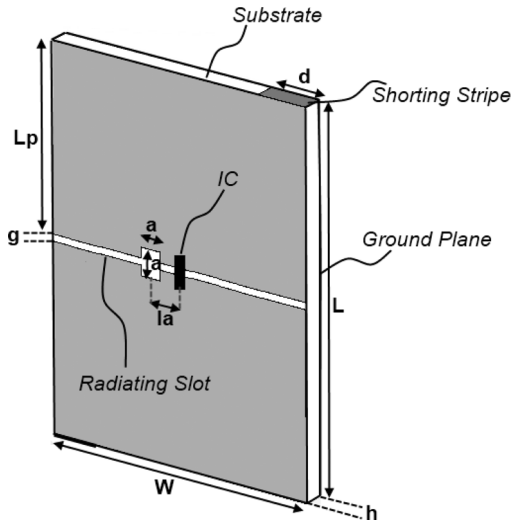

Fig. 1. Layout of the miniaturized sensor tag. The chemically interactive material (CIM) will be deposited inside a $a \times a$ niche along the radiating slot.

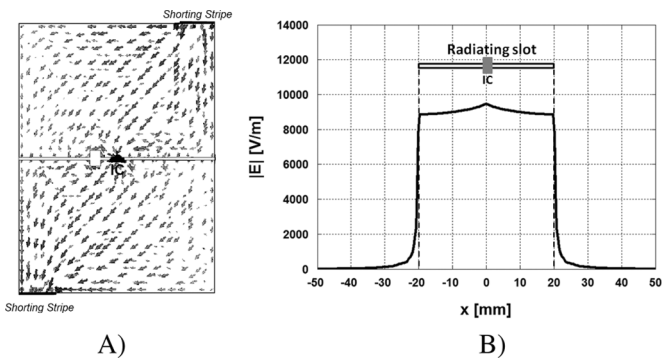

Fig. 2. (A) Typical paths of electric current lines over the top surface of the tag (size as in Table I) which are lengthened by the two opposite adjustable shorting stripes. (B) Absolute value of the electrical aperture field along the slot line (x direction) in absence of the niche.

in absence of the CIM. The two possible utilizations of the doped tag are described in detail in Sections V and VI through application to humidity detection by means of PEDOT:PSS loading. Finally, the capability of the tag and the comparison of its performance with the state of the art are discussed in the Conclusion.

II. Antenna Layout

The antenna layout is composed of two coplanar patches of size $\{W, L_p\} < \lambda/4$ forming an open-circuit nonresonant slotline, as shown in Fig. 1. The RFID microchip is placed in the middle of the radiating slot. The opposite corners of the two patches are connected to the ground plane by means of two thin vertical stripes so that the current path is lengthened along the overall diagonal [Fig. 2(A)] with great benefit to antenna miniaturization. The resonance frequency is hence mostly determined by the length $\sqrt{(2L_p)^2 + W^2}$ of the diagonal, the maximum gain is related to the width W of the layout. A fine tuning of the operating frequency is possible by acting on the size d of the shorting vertical stripes, in order to produce a frequency shift of the tag's resistance and reactance.

Since $W < \lambda/4$, the open-circuit slot hosts a strong and slowly variable aperture-field, as shown in Fig. 2(B) and hence

TABLE I
Size in Millimeters of the Parameters in Fig. 1

Parameter	Value [mm]
L	55
Lp	27
W	40
g	1
a	3
d	7.5
g	1
h	3
la	4.5

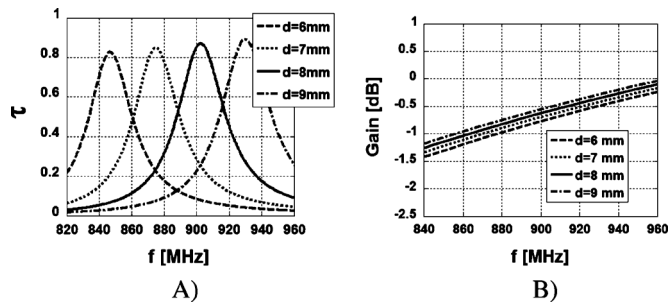

Fig. 3. Parametric analysis of the power transmission coefficient (A) and gain (B) of the unloaded tag, obtained by FDTD simulations, for some widths d of the shorting stripes (Fig. 1), having fixed the other sizes of the tag as in Table I.

it is the most sensitive part of the antenna, suitable to contain the sensor which will be deposited into a niche close to the microchip. The radiation diagram is expected to be broadside.

All the electromagnetic simulations have been performed by the Finite-Difference Time-Domain (FDTD) method in the CST Microwave Studio 2012 implementation. The RFID antenna has been simulated in free space by using the transient solver delivering broadband frequency domain results such as input impedance and gain. Fig. 3(A) shows a parametric simulation of the power transfer coefficient τ of the tag, defined as

$$\tau = 1 - |\Gamma|^2 = \frac{4R_c R_A}{|Z_c + Z_A|^2} \leq 1 \tag{1}$$

with $Z_A = R_a + jX_a$ the input impedance of the antenna and $Z_C = 25 - j237\ \Omega$ the equivalent RF impedance of a reference commercial microchip transponder *NXP G2il* IC [17] with power sensitivity $p_C = -18$ dBm. The antenna is assumed to include a 3-mm-thick Forex slab as substrate with parameters $\epsilon = 1.55, \sigma = 6 \cdot 10^{-4}$ S/m. The external size is 40 mm × 55 mm, e.g., half the surface of a credit card, corresponding to $0.12 \cdot \lambda \times 0.15 \cdot \lambda$ at 868 MHz; detailed dimensions are listed in Table I. Variations of the width d of the shorting stripes produce a significant monotonic and linear frequency shift of the power transfer coefficient as large as 30 MHz/mm, with a slight but negligible change in the peak value. The gain of the tag [Fig. 3(B)] is instead much less sensitive to the change of d, so that the profile of the realized gain of the tag, with respect to the control parameter, is mostly related to the frequency shift of the power transfer coefficient.

The peak of the power transfer coefficient is quite stable $(0.8 < \tau < 0.9)$ for 6 mm $\leq d \leq$ 9 mm and hence the antenna may be tuned to European RFID band (866–869 MHz) or USA band (902–928 MHz) by just small geometrical changes. In practical applications, the size of the stripes can be easily

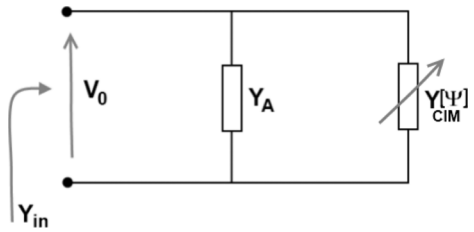

Fig. 4. Slotline's equivalent circuit model with the CIM equivalent admittance $Y_{\mathrm{CIM}}[\Psi]$ in parallel to the input admittance of the unloaded antenna Y_A.

modified by adding or removing narrow pieces of adhesive copper.

III. Lumped Element Model of the Doped Tag

Let Ψ denotes the concentration of the gas that has to be monitored by the radio-sensor. The electromagnetic effect of the chemical interaction between such a gas and the CIM sensor can be considered as a perturbation to the gain and to the input impedance of the sensor-less antenna. Due to the very small size of the niche ($a \sim \lambda/100$), the loaded CIM can be taken into account as a lumped variable admittance $Y_{\mathrm{CIM}}[\Psi] = g_{\mathrm{CIM}}[\Psi] + j \cdot B_{\mathrm{CIM}}[\Psi]$. Moreover, since the electromagnetic field inside the slot-line is expected to be nearly uniform [as previously shown in Fig. 2(B)], the CIM admittance can be considered as interconnected (Fig. 4) in parallel to the admittance $Y_A = g_A + j \cdot B_A$ of the unloaded (blank) antenna estimated by simulations or measurements at the position of the RFID chip.

The input admittance of the loaded tag $Y_{\mathrm{in}}[\Psi] = Y_A + Y_{\mathrm{CIM}}[\Psi]$ is definitely dependent on the concentration Ψ of the gas under observation. It is now useful to express the performance indicator of an RFID tag, e.g., the realized gain

$$\hat{G_\tau}(\theta, \varphi)[\Psi] = G(\theta, \varphi)[\Psi] \cdot \tau[\Psi] \tag{2}$$

in terms of the equivalent admittance of the CIM loading.

From Fig. 4, the input power of the unloaded tag can be expressed as

$$P_A = \frac{1}{2} g_A \left| V_0^2 \right| \tag{3}$$

while the power absorbed in the sensing load, is

$$P_{\mathrm{CIM}}[\Psi] = \frac{1}{2} g_{\mathrm{CIM}}[\Psi] \left| V_0^2 \right|. \tag{4}$$

The gain of the loaded antenna can be calculated as

$$G(\theta, \varphi)[\Psi] = 4\pi \frac{I(\theta, \varphi)}{P_A + P_{\mathrm{CIM}}[\Psi]} = \alpha[\Psi] G_0(\theta, \varphi) \tag{5}$$

where $I(\theta, \varphi)$ is the radiation intensity, $G_0(\theta, \varphi)$ is the gain of the unloaded tag, and

$$\alpha[\Psi] = \frac{g_A}{g_A + g_{\mathrm{CIM}}[\Psi]} < 1 \tag{6}$$

is the degradation of the gain introduced by the chemical perturbation, which will negatively impact on the read-range performance of the sensor tag.

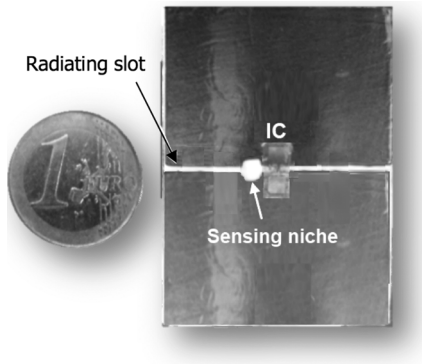

Fig. 5. Top view of the RFID sensor prototype over a 3-mm-thick Forex substrate.

The power transmission coefficient of the loaded tag can be hence deduced from (1) by substitution $Z_{\mathrm{in}}[\Psi] = (Y_A + Y_{\mathrm{CIM}}[\Psi])^{-1}$, and $Z_C = Y_C^{-1}$, so that

$$\tau[\Psi] = \frac{4 g_C (g_A + g_{\mathrm{CIM}}[\Psi])}{\left| Y_C + Y_A + Y_{\mathrm{CIM}}[\Psi] \right|^2}. \tag{7}$$

The realized gain of the CIM-loaded tag is hence finally calculated from (2), (5), and (7), where also the dependence on the tuning parameter d (Fig. 1) is made explicit, as

$$\hat{G_\tau}[d, \Psi] = G_0[d] \cdot \left(1 - \frac{g_{\mathrm{CIM}}[\Psi]}{g_A[d]}\right)^{-1} \frac{4 g_C (g_A[d] + g_{\mathrm{CIM}}[\Psi])}{\left| Y_C + Y_A[d] + Y_{\mathrm{CIM}}[\Psi] \right|^2} \tag{8}$$

where the angular dependence has been omitted for notation simplicity. As shown later on, the above model can be used to estimate the equivalent admittance $Y_{\mathrm{CIM}}[\Psi]$ of the CIM at different grades of gas concentration. The estimation can be done by means of a parameter-identification procedure aimed at projecting measured data over (8). In other words, this family of RFID tags may become the base for a dynamical radio frequency characterization of chemical receptors in realistic conditions. Once the CIM has been characterized through the equivalent admittance, the same (8) can be hence used, in conjunction to Fig. 3, to predict and shape the overall antenna response. The peak gain can be moved to the most convenient frequency of the RFID band by acting on the control parameter d. Accordingly, the reader-tag interaction will permit to appreciate the largest dynamic range of the sensing process, while preserving the minimum required communications performances. Some operative examples of tuning agility are given in Section V.

IV. Prototype

A prototype of the miniaturized sensor tag (Fig. 5) has been fabricated with the same sizes as in Table I by properly carving and wrapping an adhesive copper sheet on the Forex substrate.

The communication performance of the unloaded tag has been characterized in terms of realized gain. Measurements have been performed by means of a UHF long-range reader based on the ThingMagic M5 ASIC, whose output power can be controlled by 0.5-dBm steps in the frequency range 840–960 MHz. The reader's antenna is a 5-dB linear polarized

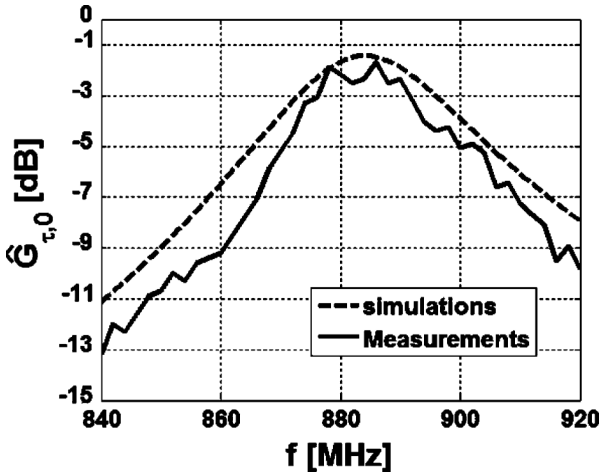

Fig. 6. Measured and simulated realized gain along the antenna's broadside direction for the unloaded ("blank") sensor tag of Fig. 5.

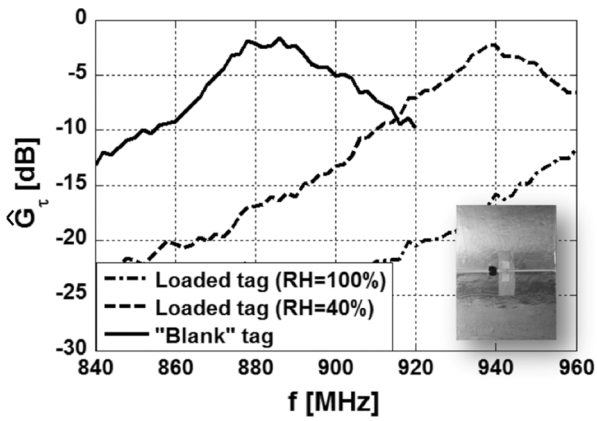

Fig. 7. Measured realized gain in the broadside direction for the chemical-loaded and "blank" tags. Measurements have been performed within the range of frequencies allowed by the reader (840 MHz–960 MHz).

patch, placed 50 cm away from the radio-sensor. It is worth clarifying that, even if the following simulated and measured diagrams are given in the whole frequency range allowed by the reader (that includes all the World RFID band) at the purpose to better understand the physical phenomena, the proposed sensing methodology is intrinsically narrowband because of the strong local frequency limitations, especially in Europe (866–869 MHz). A single-frequency characterization, useful for real sensing purpose, will be instead presented in Section VI.

Once known the reader gain G_R, the reader-tag distance d, the polarization factor η_p between the reader and the tag and the measured turn-on power $P_{\rm in}^{\rm to}$, e.g., the minimum input power required by the reader's unit to activate the remote microchip to send back its code, the realized gain is estimated [18] by

$$\hat{G}_{\tau,0} = \left(\frac{4\pi d}{\lambda_0}\right)^2 \frac{P_{\rm chip}}{G_R P_{\rm in}^{\rm to} \eta_p}. \tag{9}$$

The corresponding results are shown in Fig. 6 in comparison with FDTD simulations. By considering 3.2 W EIRP, the maximum emitted power from the reader allowed by European regulations and a circular polarized reader's antenna ($\eta_p = 0.5$), the estimated free-space maximum read range [from (9)] is about 7 m.

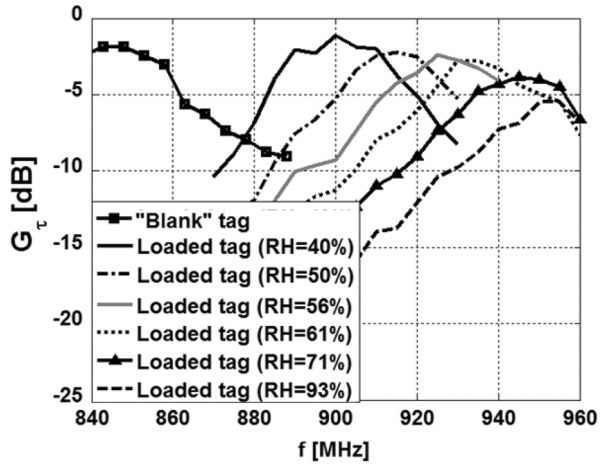

Fig. 8. Measured realized gains of the retuned ($d = 6.5$ mm) "blank" and chemical-doped tags in the broadside direction for different levels of humidity.

V. CIM Loading Characterization and Effects

The tag's capability to be used in the electromagnetic characterization of CIMs is now discussed and demonstrated by exposing the tag to humidity variations. The chemical interactive material is Pedot:PSS painted in the sensing niche (the black pixel in the inset of Fig. 7). The strongly hygroscopic polymer, in its commercial form Clevios PH 500 [19], absorbs moisture almost instantaneously when handled under ambient conditions [16]. By using just a single polymer drop inside the sensing niche (Fig. 7), a highly sensitive passive humidity sensor can be achieved, as shown later on.

The measured realized gain of the chemical loaded tag for two different grades of relative humidity (RH), e.g., ambient level ($\mathrm{RH} = 40\%$) and saturation ($\mathrm{RH} = 100\%$), are compared with that of the "blank" tag. The humidity saturation has been obtained by placing the tag inside a closed plastic chamber partially filled with water [8]. The presence of the polymer induces a significant frequency shift of the tags' response towards higher frequencies with respect to the blank configuration and such a shift is proportional to the grade of humidity. The peak value of the gain of the loaded tag at humidity saturation (100%) overcomes the frequency limit of the reader (960 MHz) and therefore it cannot be appreciated by the measurement.

In order to evaluate the effects of the CIM in the whole considered range of humidity (40% to 100%), the loaded tag has been manually retuned to keep the operative frequency of the tag around 900 MHz. Starting from the tuning chart in Fig. 3, the requested 35 MHz shift towards lower frequencies in condition of ambient humidity has been practically achieved by reducing the length d of the shorting strip lines from 7.5 to 6.5 mm. The new measured realized gains of the retuned chemical-loaded tag for different levels of humidity can be now fully appreciated by the reader (in Fig. 8), and the system is now ready to estimate the equivalent CIM parameters.

The dielectric properties of PEDOT:PSS have been characterized for a first time at radio frequencies by the same authors in [8] where the conductive polymer was simply considered as a "lossy metal." Here, a more complete model of the CIM is considered by accounting also for the capacitive effects due to the water absorption into the Pedot:PSS. The assumed equivalent

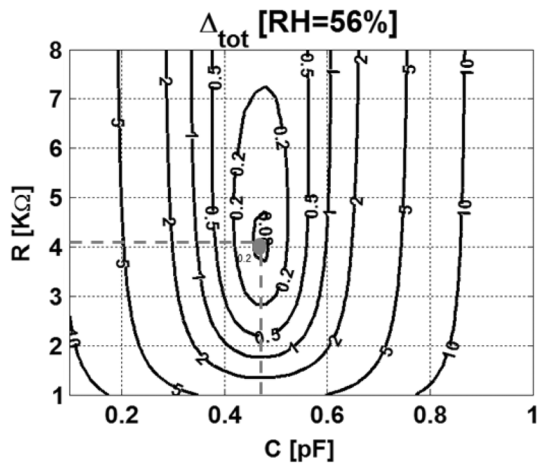

Fig. 9. Isolines of the global error $\Delta_{\rm tot}[{\rm RH}=56\%]$ for the parametric identification of the equivalent resistance $R_{\rm CIM}$ and capacitance $C_{\rm CIM}$ (Fig. 4) of the PEDOT:PSS drop corresponding to the humidity ${\rm RH}=56\%$. The gray circle indicates the couplet $(R_{\rm CIM}, C_{\rm CIM})$ minimizing the error in (10).

admittance of the CIM is hence a parallel connection of a Resistance and a Capacitance $\{R_{\rm CIM}[{\rm RH}_n],\ C_{\rm CIM}[{\rm RH}_n]\}$ whose values at discrete humidity grades $\{{\rm RH}_n\}$ are here identified with the following procedure involving the lumped model considered in (8).

i) The realized gain $G^{\rm meas}_{\tau,f_i}[{\rm RH}_n]$ of the loaded tag is measured at some frequencies $\{f_i\}$, in several different humidity concentration, starting from ambient air (${\rm RH}=40\%$) up to fully wet air (${\rm RH}=100\%$), as previously shown in Fig. 8;
ii) the input impedance $(Z_A=(1)/(Y_A))$ and the gain (G_0) of the unloaded tag are obtained by FDTD simulations;
iii) the lumped model $G^{\rm mod}_{\tau,f_i}(R_{\rm CIM}[{\rm RH}_n], C_{\rm CIM}[{\rm RH}_n])$ in (8) is finally inverted to identify the unknown parameters of the CIM by minimizing, at every considered humidity concentration ${\rm RH}_n$, the following error function:

$$\Delta_{\rm tot}[{\rm RH}_n] = \sum_{i=1}^{3} \frac{\left|G^{\rm meas}_{\tau,f_i}[{\rm RH}_n] - G^{\rm mod}_{\tau,f_i}(R_{\rm CIM}[{\rm RH}_n], C_{\rm CIM}[{\rm RH}_n])\right|^2}{\left|G^{\rm meas}_{\tau,f_i}[{\rm RH}_n]\right|^2} \tag{10}$$

with $f_i=\{f_{G\ \max,{\rm RH}n},\ f_{G\max,RH\ n}\pm 10\ {\rm MHz}\}$, where $f_{\rm Gmax,RHn}$ refers to the frequency corresponding to the peak of the measured realized gain of the loaded sensor at the considered humidity level ${\rm RH}_n$.

An example of parameter identification of the PEDOT:PSS resistance $R_{\rm CIM}[{\rm RH}_n]$ and capacitance $C_{\rm CIM}[{\rm RH}_n]$ is shown in Fig. 9, where the error isolines $\Delta_{\rm tot}$ obtained from (10) are referred to the humidity ${\rm RH}=56\%$.

The estimated values of $C_{\rm CIM}[{\rm RH}_n]$ and $R_{\rm CIM}[{\rm RH}_n]$ as a function of the humidity grade from 40% to 100% are summarized in Fig. 10. The obtained samples for both resistance and capacitance have been fitted by a mean-square interpolation, using a second-order polynomial

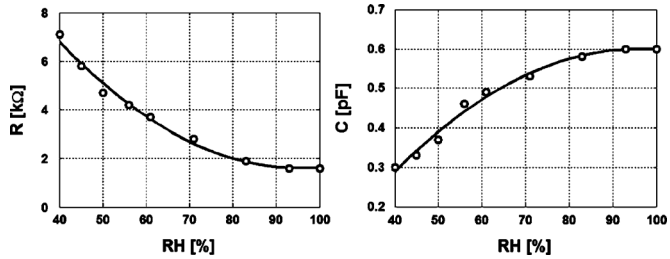

Fig. 10. Estimated values (circles) of the capacitance $C_{\rm CIM}$ and resistance $R_{\rm CIM}$ of Pedot:PSS for different levels of humidity between 40% and 100%. The data have been fitted by a second-order mean square interpolation (continuous lines).

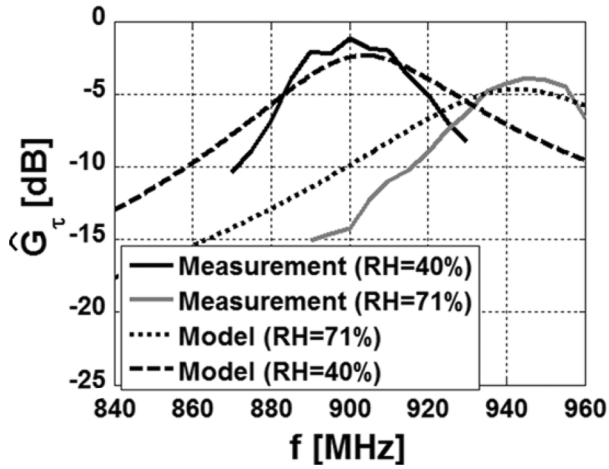

Fig. 11. Measured and estimated realized gain for two different RH levels along the antenna axis (broadside observation) by using the identified values of capacitance $C_{\rm CIM}$ and resistance $R_{\rm CIM}$ of the Pedot:PSS load.

$$\begin{bmatrix} R_{\rm CIM}[{\rm RH}] \\ C_{\rm CIM}[{\rm RH}] \end{bmatrix} \simeq \sum_{k=0}^{2} \begin{bmatrix} a_{R,k} \\ a_{C,k} \end{bmatrix} {\rm RH}^k \tag{11}$$

with $\{a_{R,k}\}_{k=0\cdots 2} = \{17,\ -0.32,\ -1.7\cdot 10^{-4}\}$, and $\{a_{C,k}\}_{k=0\ldots 2} = \{-0.31,\ 0.02,\ -1\cdot 10^{-4}\}$. It is clearly visible how the optimized resistance of Pedot:PSS decreases with a greater water absorption due to power loss, while the capacitance of the polymer increases because of its higher permittivity. Both the values tend to saturate close to ${\rm RH}=100\%$.

For a cross-check, Fig. 11 compares the measured and calculated realized gains at two humidity levels ${\rm RH}=\{40\%, 71\%\}$ showing a satisfactory agreement nearby the peaks of the tags responses.

VI. Design Example: Optimized Humidity Sensor

Having estimated the PEDOT:PSS equivalent lumped parameters $\{R_{\rm CIM}, C_{\rm CIM}\}$, the model of (8) is now applied to optimize the sensitivity of the PEDOT:PSS-loaded tag to humidity, at the RFID European frequency ${\rm f}=868$ MHz, by properly modifying the geometrical parameter d of the tag. The equivalent admittance $Y_{\rm CIM}[{\rm RH}]$ of Pedot:PSS is estimated by (11), while the input impedance $Y_A[d]$ and the gain $G_0[d]$ of the unloaded tag are obtained by FDTD simulations. By

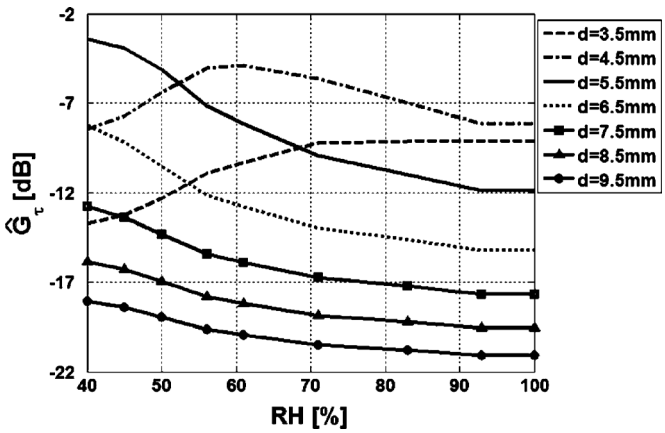

Fig. 12. Estimated values of the sensor tag's realized gains $\hat{G}_\tau[d, \mathrm{RH}]$ at 868 MHz according to the model in (8).

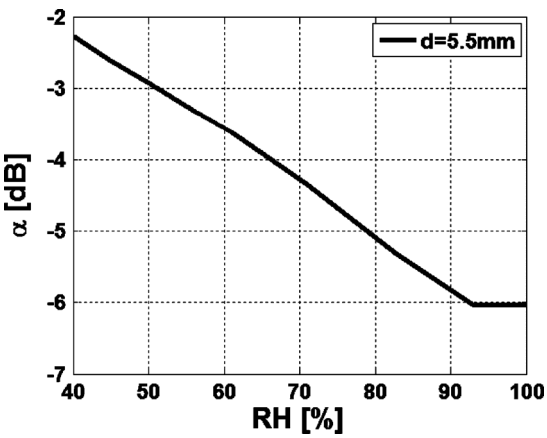

Fig. 13. Estimated values of the gain degradation factor (6) at 868 MHz caused by the chemical loading.

representing (Fig. 12) the predicted realized gain $\hat{G}_\tau[d, \mathrm{RH}]$ of the Pedot:PSS-loaded tag with respect to increasing humidity concentrations, it is clearly evident that the slope of the curves (corresponding to the device's sensitivity) and their absolute value may be tuned by adjusting the size d of the shorting stripes. In particular, the choice $d = 5.5$ mm permits to achieve the best compromise between the absolute value of realized gain all along the RH variation (affecting the read range), the sensitivity to RH, the dynamic range and finally the monotonicity of the $\mathrm{RH} \leftrightarrow \hat{G}_\tau$ profile. In this case, the gain degradation factor defined in (6) is $\alpha[\mathrm{RH} = 40\% \cdots 100\%] = 3.5$ dB (Fig. 13) and therefore the span of dynamic range of the tag response in Fig. 12 is mostly imposed by the impedance mismatch, e.g., by the change of τ.

The performance of the retuned sensor ($d = 5.5$ mm) are finally characterized at fixed frequency $\mathrm{f} = 868$ MHz during dynamic exposures to humidity and subsequent recovery in order to evaluate the real achievable dynamic ranges, sensitivities and hysteresis as in [8].

The considered metrics are the turn-on power $P_{\mathrm{to}}^{\mathrm{in}}[\mathrm{RH}]$, the backscattered power $P_{\mathrm{BS}}[\mathrm{RH}]$ and the Analog Identifier. The backscattered power is deduced from the received signal strength indicator (RSSI), provided by the reader, and then

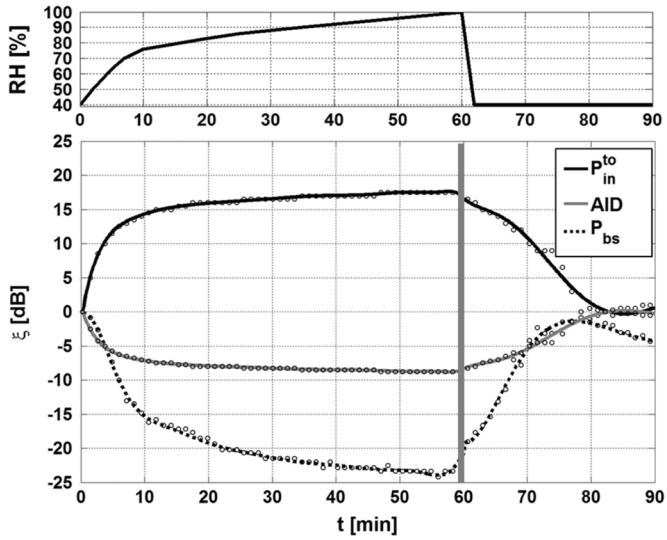

Fig. 14. (Top) Measured variation of relative humidity during one hour exposure from ambient air ($\mathrm{RH} = 40\%$) to saturated air ($\mathrm{RH} = 100\%$) and 30 minutes recovery, as measured by a digital hygrometer. (Bottom) Sensing curves at 868 MHz normalized with respect to the initial value, e.g., at ambient RH. Data (circles) have been fitted by a mean square interpolation.

TABLE II
SENSITIVITIES [dB/RH] OF MEASURED TURN-ON POWER, BACKSCATTER POWER AND ANALOG IDENTIFIER

	$RH_{low}-RH_{high}$	[dB/RH]
$S[P_{in}^{to}]$	$40\% - 80\%$	0.39
	$80\% - 100\%$	0.08
$S[AID]$	$40\% - 80\%$	0.19
	$80\% - 100\%$	0.08
$S[p_{BS}]$	$40\% - 80\%$	0.44
	$80\% - 100\%$	0.28

transformed through the following conversion rule (specific for the used reader)

$$P_{\mathrm{BS}} = 0.8\ \mathrm{RSSI} + 24 - G_{\mathrm{LNA}} - 96 - 0.8\ \mathrm{RSSI}_{\mathrm{th}} \qquad (12)$$

with $\mathrm{RSSI}_{\mathrm{th}} = 48$ and G_{LNA} gain of the low noise signal amplifier, defined in the communication register. For generality, the backscattered power is normalized by the input power:

$$p_{\mathrm{BS}} = \frac{P_{\mathrm{BS}}}{P_{\mathrm{in}}} \qquad (13)$$

The analog identifier (AID) is a dimensionless parameter defined as

$$\mathrm{AID}[\mathrm{RH}] = \frac{P_{\mathrm{chip}}}{\sqrt{P_{\mathrm{in}}^{\mathrm{to}}[\mathrm{RH}] P_{R\leftarrow T}[\mathrm{RH}]}} = \sqrt{\tau \frac{R_C}{R_{\mathrm{in}}}} = \sqrt{\tau \frac{(R_A + R_{\mathrm{CIM}}) R_C}{R_A R_{\mathrm{CIM}}}} \qquad (14)$$

which can be computed from measurements [7] starting from the above powers and permits angle and distance-independent measurements.

Fig. 14 shows the measured normalized variation of the sensing indicators for a single 1.5-h cycle of exposure/recovery. Measured data are interpolated by mean-square.

TABLE III
COMPARISON OF THE PROPOSED RADIO SENSOR'S PERFORMANCE TO SOME STATE-OF-THE-ART HUMIDITY PASSIVE SENSORS

Ref. >>	[10]	[11]	[8]	[13]	Proposed Tag
External area $[cm^2]$	49	42	52	30	22
Realized Gain [dB]	-	-3	-3	-	-1.5
Turn-on Power Sensitivities $[dB/RH]RH \in [40\% - 80\%]$	0.12	0.02	0.13	0.13	0.39
CIM	Blotting paper	Kapton Substrate	Pedot:PSS	Kapton Tape	Pedot:PSS, just one drop

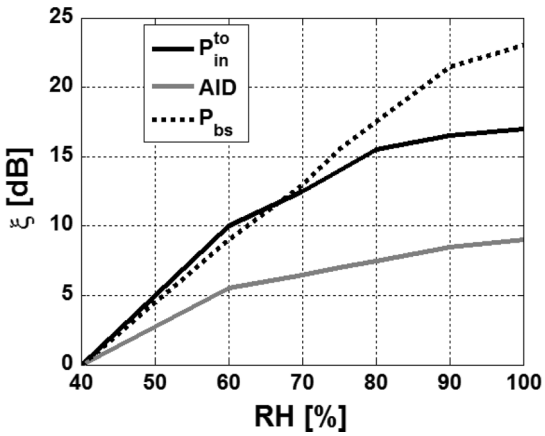

Fig. 15. Calibration curves of the RFID sensor from Fig. 14. Turn-on power and backscattered power are represented as a function of humidity.

The change of the response curves follows the exponential humidity profile with dynamic ranges for turn-on power, backscattered power and AID of 17, 23, and 9 dB, respectively. These values are higher than those predicted by the model as the parameter identification of Y_{CIM} is less accurate for frequencies far from the gain's peaks, as visible in Fig. 12. The recovery process down to the ambient humidity $(\mathrm{RH} = 40\%)$, right after the end of humidity exposure, takes around 30 min, even if just 20 min are enough for the sensor to recover almost completely. The hysteresis is less than 1 dB.

Finally, Fig. 15 shows the *Calibration Curves*, e.g., the sensor responses as a function of moisture, normalized with respect to the initial condition. The profiles appear almost linear for the backscattered power, while the turn-on power saturates for humidity levels greater than 80%.

The sensitivity of the device, defined as the power difference generated by 1% change in the RH level, can be extracted as the slope of the linearized curves of Fig. 15

$$S[\xi] = \frac{|\Delta\xi|}{|\Delta\mathrm{RH}|} = \frac{|\xi(\mathrm{RH_{high}}) - \xi(\mathrm{RH_{low}})|}{|\mathrm{RH_{high}} - \mathrm{RH_{low}}|}. \qquad (15)$$

The sensitivity values for the indicators of Fig. 15 are listed in Table II.

The backscattered power metric appears as the most sensitive indicator to humidity change with 0.44 dB/RH sensitivity between 40% and 80% relative humidity. The analog identifier, even if less sensitive than other indicators, is however very interesting since it does not require an accurate control of the measurement setup and it is hence the right choice for mobile readers.

VII. DISCUSSIONS AND CONCLUSION

The proposed planar tag revealed as a simple, highly sensitive and tunable miniaturized device, suitable to be used as a gas sensor. The tuning mechanism is agile, easily accessible and it enables a custom shift of the tag response at any frequency in the global RFID band, without demanding for significant geometrical modifications. The equivalent lumped-element model of the chemical loading can be used to predict the sensor's response to the gas exposure, as well as to characterize the electrical properties of the CIM.

When loaded with PEDOT:PSS for the detection of humidity concentration, the sensor is able to provide up to 0.4 dB/RH sensitivity at the cost of just a single polymer drop deposited right next to the microchip. Moreover, the water absorption is mostly completely reversible, as shown in Fig. 14, and multiple measurements demonstrated a good repeatability at different days and conditions. It is finally worth comparing the size and sensitivity of the proposed RFID humidity sensor to that of state-of-the-art passive UHF humidity sensors (Table III). The proposed layout is capable to exhibit up to three-times larger sensitivity than the other devices, while requiring half the surface area. Moreover, the antenna is completely unspecific and could be doped by other chemical interactive materials properly functionalized in order to react to different gases. Encouraging experiments are currently being run by the authors with carbon nanotubes to sense ammonia and other kind of polymers.

It is finally worth noting that CIMs generally suffer from cross-sensitivity, e.g., they could react to multiple volatile compounds. Thus, the single device should be used in case a unique and known volatile species is present, as it happens in some controlled industrial processes. For a more general and uncontrolled applications, instead, this class of RFID sensors can be arranged within a sensor array forming a radio-chemical nose. Each tag of the array will be doped by different CIMs in order to setup a classification procedure able to identify and quantify

each volatile specie in the environment. This is the subject of running research.

ACKNOWLEDGMENT

The authors would like to thank Prof. C. Di Natale and Dr. A. Catini for very valuable support and discussions about CIM and sensors' characterization.

REFERENCES

[1] L. Atzori, A. Iera, and G. Morabito, "The internet of things: A survey," *Comput. Netw.*, vol. 54, no. 15, pp. 2787–2805, 2010.
[2] V. Jelicic, M. Mango, D. Brunelli, G. Paci, and L. Benin, "Design, characterization and management of a wireless sensor network for smart gas monitoring," in *Proc. 4th IEEE Int. Workshop Adv. Sens. Interfaces (IWASI)*, Jun. 2011, pp. 115–120.
[3] V. Jelicic, M. Mango, D. Brunelli, G. Paci, and L. Benin, "A context-adaptive multimodal wireless sensor network for energy-efficient gas monitoring," *IEEE Sens. J.*, vol. 13, no. 1, pp. 328–338, Jan. 2013.
[4] Y. Wang and J. T. W. Yew, "A review of carbon nanotubes-based gas sensors," *J. Sens.*, vol. 2009, pp. 24–, 2009, Article ID 493904.
[5] T. T. Thai, L. Yang, G. R. DeJean, and M. M. Tentzeris, "Nanotechnology enables wireless gas sensing," *IEEE Microw. Mag.*, vol. 12, no. 4, pp. 84–95, Jun. 2011.
[6] R. Vas, V. Lakafosis, L. Hose, G. Shaker, L. Yang, G. Orecchini, A. Trail, M. M. Tentzeris, and L. Rosalie, "Inkjet printed, self powered, wireless sensors for environmental, gas, and authentication-based sensing," *IEEE Sens. J.*, vol. 11, no. 12, pp. 3139–3152, Dec. 2011.
[7] G. Marrocco, "Pervasive electromagnetic: Sensing paradigms by passive RFID technology," *IEEE Wireless Commun.*, vol. 17, no. 6, pp. 10–17, Dec. 2010.
[8] S. Manzari, C. Occhiuzzi, S. Newell, A. Catini, C. Di Natale, and G. Marrocco, "Humidity sensing by polymer-loaded UHF RFID antennas," *IEEE Sens. J.*, vol. 12, no. 9, pp. 2851–2858, Sep. 2012.
[9] C. Occhiuzzi, A. Rida, G. Marrocco, and M. Tentzeris;, "RFID passive gas sensor integrating carbon nanotubes," *IEEE Trans. Microwave Theory and Techniques*, vol. 59, no. 10, pp. 2674–2684, 2011, Part: 2.
[10] J. Siden, G. Jinlan, and B. Neubauer, "Microstrip antennas for remote moisture sensing using passive RFID," in *Asia-Pacific Microw. Conf., Singapore*, Dec. 2009, pp. 2375–2378.
[11] J. Virtanen, L. Ukkonen, T. Bjorninen, A. Z. Elsherbeni, and L. Sydnheimo, "Inkjet-printed humidity sensor for passive UHF RFID systems," *IEEE Trans. Instrum. Meas.*, vol. 60, no. 8, pp. 2768–2777, Aug. 2011.
[12] R. Nair, E. Perret, S. Tedjini, and T. Barron, "A humidity sensor for passive chipless RFID applications," in *Proc. IEEE Int. Conf. RFID—Technol. Applicat. (RFID—TA)*, 2012, pp. 29–33.
[13] E. M. Amin and N. C. Karmakar, "Development of a low cost printable humidity sensor for chipless rfid technology," in *Proc. IEEE Int. Conf. RFID—Technol. Applicat. (RFID—TA)*, 2012, pp. 165–170.
[14] T. Blythe and D. Bloor, *Electrical Properties of Polymers*, 2nd ed. Cambridge, U.K.: Cambridge Univ. Press, 2005.
[15] S. Manzari, A. Catini, C. Di Natale, and G. Marrocco, "Ambient sensing by chemical-loaded UHF-RFIDs," in *Proc. 7th Eur. Conf. Antennas Propag. (EuCAP)*, Apr. 2013, pp. 1718–1720.
[16] A. Elschner, S. Kirchmeyer, W. Lovenich, U. Merker, and K. Reuter, *PEDOT: Principles and Applications of an Intrinsically Conductive Polymer*. Boca Raton, FL, USA: CRC Press, Taylor and Francis Group, LLC, 2011.
[17] References NXP G2il Datasheet, [Online]. Available: http://www.nxp.com
[18] G. Marrocco and F. Amato, "Self-sensing passive RFID: From theory to tag design and experimentation," in *Proc. 39th Eur. Microw. Conf.*, Sep. 2009, pp. 1–4.
[19] Clevios PH500, [Online]. Available: http://clevios.com

Sabina Manzari was born in Rome, Italy, in 1985. She received the M.Sc. degree (with honors) in medical engineering from the University of Rome "Tor Vergata," Rome, Italy, in 2010, where she is currently pursuing the Ph.D. degree in geoinformation.

Her research interests include electromagnetism, passive RFID chemical sensors, and wireless health monitoring by means of wearable radio frequency identification techniques. In 2010–2011, she was a Visiting Researcher in the RFID Research Group, Tampere University of Technology (Finland). Her research was mainly focused in passive RFID sensors development for temperature and heat monitoring.

Gaetano Marrocco received the Laurea degree in electronic engineering and the Ph.D. degree in applied electromagnetics from the University of L'Aquila, L'Aquila, Italy, in 1994 and 1998, respectively.

He is currently an Associate Professor of Electromagnetics at the University of Rome "Tor Vergata," Rome, Italy, where he directs the Pervasive Electromagnetics Lab. His research is mainly focused to the radio frequency identification technology, to body-centric systems, wireless chemical and mechanical sensors and to the ambient intelligence. He has been moreover involved in several programs of the European Space Agency, NATO, and Finmeccanica concerning distributed antenna systems over ships, satellites, and airplanes.

Prof. Marrocco serves as Associate Editor of the IEEE ANTENNAS AND WIRELESS PROPAGATION LETTERS, Associate Editor of the IEEE RFID Virtual Journal, Vice-Chair of the Italian delegation URSI Commission D: Electronics and Photonics. He was the co-chair of the RFIDays-2010 International Workshop in Finland, Chairman of the Local Committee of the V European Conference on Antennas and Propagation (EUCAP-2011), TPC chair of the 2012 IEEE-RFID TA in Nice, France and TPC co-Chair of the 2013 IEEE-RFID USA. He is the cofounder and President of the University spin-off RADIO6ENSE active in the short-range electromagnetic sensing for Aerospace, Healthcare, Internet of Things and Smart Cities.